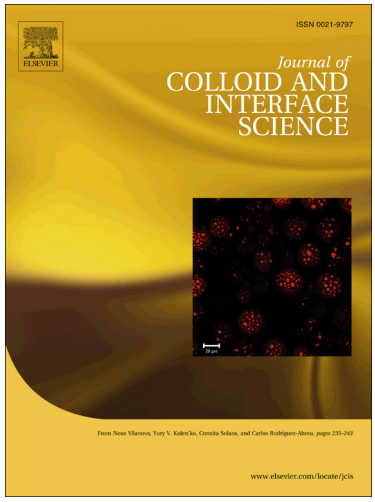

A GCMC Simulation and Experimental Study of Krypton Adsorption/Desorption Hysteresis on a Graphite Surface

Luisa Prasetyo, Toshihide Horikawa, Poomiwat Phadungbut, Shiliang (Johnathan) Tan, D.D. Do, D. Nicholson

PII: S0021-9797(16)30392-7
DOI: http://dx.doi.org/10.1016/j.jcis.2016.06.033
Reference: YJCIS 21343

To appear in: *Journal of Colloid and Interface Science*

Received Date: 11 April 2016
Revised Date: 10 June 2016
Accepted Date: 11 June 2016

Please cite this article as: L. Prasetyo, T. Horikawa, P. Phadungbut, S. (Johnathan) Tan, D.D. Do, D. Nicholson, A GCMC Simulation and Experimental Study of Krypton Adsorption/Desorption Hysteresis on a Graphite Surface, *Journal of Colloid and Interface Science* (2016), doi: http://dx.doi.org/10.1016/j.jcis.2016.06.033

A GCMC Simulation and Experimental Study of Krypton Adsorption/Desorption Hysteresis on a Graphite Surface

Luisa Prasetyo[a], Toshihide Horikawa[b], Poomiwat Phadungbut[c], Shiliang (Johnathan) Tan[a], D. D. Do[a] and D. Nicholson[a]

[a]School of Chemical Engineering
University of Queensland
St. Lucia, Qld 4072
Australia

[b]Department of Advanced Materials, Institute of Technology and Science
The University of Tokushima
2-1 Minamijosanjima, Tokushima 770-8506
Japan

[c]School of Chemical Engineering
Suranaree University of Technology
Nakhon, Ratchasima, 30000
Thailand

Abstract

Adsorption isotherms and isosteric heats of krypton on a highly graphitized carbon black, Carbopack F, have been studied with a combination of Monte Carlo simulation and high-resolution experiments at 77K and 87K. Our investigation sheds light on the microscopic origin of the experimentally observed, horizontal hysteresis loop in the first layer, and the vertical hysteresis-loop in the second layer, and is found to be in agreement with our recent Monte Carlo simulation study[1]. From detailed analysis of the adsorption isotherm, the latter is attributed to the compression of an imperfect solid-like state in the first layer, to form a hexagonally packed, solid-like state, immediately following the first order condensation of the second layer. To ensure that capillary condensation in the confined spaces between microcrystallites of Carbopack F does not interfere with these hysteresis loops, we carried out simulations of krypton adsorption in the confined space of a wedge-shaped pore that mimics the interstices between particles. These simulations show that, up to the third layer, any such interference is negligible.

*Corresponding author: d.d.do@uq.edu.au

TOC Graphic

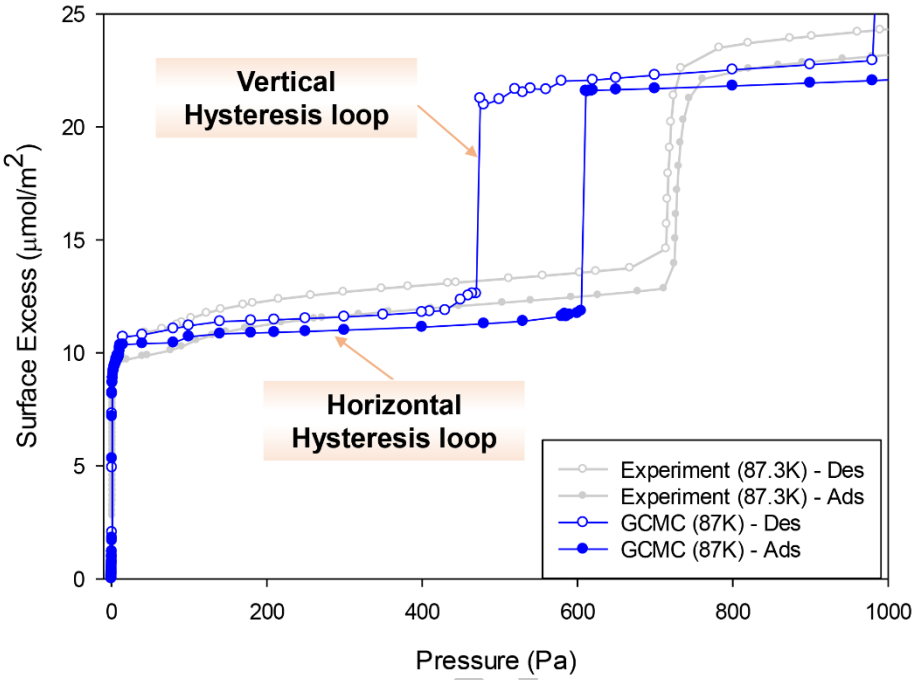

1. Introduction

The multilayer adsorption of simple gases on a highly uniform nonporous graphitic surface has been well studied [2-5] and is typically classified as a reversible Type VI isotherm according to the 2015 IUPAC classification [2] as exemplified by Ar adsorbed on highly graphitized carbon black at 77 K and 87 K [6-7]. However, experimental evidence supports the view that adsorption isotherms of ammonia [8-9], methane [10-11], carbon monoxide [12], krypton [13], xenon[14], acetone [15] and chloroform [16] on a graphite surface exhibit hysteresis at low enough temperatures. Hysteresis is normally only associated with mesoporous materials, resulting from the difference in the curvatures of the interface separating the adsorbed and gas phases along the adsorption and desorption branches of the isotherm. These unusual hysteresis loops are observed at temperatures below the bulk triple point, and disappear as the temperature increases. In their study of Xe adsorbed on graphite, Morishige *et al.*[14] attributed the hysteresis to capillary condensation in the confined spaces between micro-crystallites. Similarly, Kosugi *et al.*[13], who observed hysteresis at temperatures in the range 86.91K to 120K for krypton adsorbed on exfoliated graphite, attributed it to capillary condensation and to a liquid-solid phase transition. On the other hand, Inaba *et al.* [10], in their study of CH_4 on graphite, put forward the idea that the reason for hysteresis is an irreversible compression of the adsorbed phase which occurs as adsorption proceeds.

Our recent simulation study of Kr adsorption on a structureless graphite surface at very low temperatures[1] supports the interpretation of Inaba *et al*., showing that hysteresis occurs whenever a two-dimensional (2D) transition is observed in the grand canonical isotherm. This can be explained as a molecular rearrangement and progressive cohesiveness in the first adsorbed layer as adsorption in higher layers takes place. In the present work we examine, in greater detail, the origin of hysteresis in the adsorption isotherm for krypton on Carbopack F, a highly graphitized thermal carbon black. Our investigation comprises a combined study of high-resolution volumetric adsorption experiments and computer simulations of adsorption isotherms and isosteric heats at various temperatures, with the aim of testing the hypothesis that: if hysteresis occurs for coverages up to two layers, it may be attributed to adsorbate compression, rather than to capillary condensation.

2. Experimental

2.1 Materials

A highly graphitized thermal carbon black, Carbopack F (supplied by Supelco, USA) was used as the adsorbent. This consists of polyhedral micro-particles with homogeneous graphene layers on the faces of the polyhedra. The characteristic properties of Carbopack F have been extensively reported elsewhere [17-19]. The BET surface area is 4.9 m^2/g and there is no micropore or mesopore volume.

2.2 Measurement

Krypton adsorption on Carbopack F was measured at 77.4 K and 87.3 K using a high-resolution volumetric adsorption apparatus (BELSORP-max, MicrotracBEL). Carbopack F was degassed at 473K for 5 hours under vacuum at pressures of less than 0.1mPa to remove any physically adsorbed components before making the adsorption measurements.

2.3 Isosteric heat of adsorption

The isosteric heats of adsorption (q_{st}) for each adsorbate were calculated by applying the Clausius-Clapeyron (CC) equation to isotherm data at two temperatures (77.4 K and 87.3 K):

$$q_{st} = \frac{RT_1T_2}{T_2 - T_1} \ln\left(\frac{P_2}{P_1}\right) \quad (1)$$

where R is the gas constant, T_1 and T_2 are the adsorption temperatures and P_1 and P_2 are the respective absolute pressures at a given loading.

3. Theory

3.1 GCMC simulations

The Grand Canonical Monte Carlo (GCMC) simulations used 100,000 cycles for both equilibration and sampling stages. A few simulations were carried out with a higher number of cycles to ensure that equilibrium had been reached with the standard number. Each cycle, consisted of 1000 attempted displacement, insertion or deletion moves, chosen with equal probability. In the equilibration stage, the maximum displacement step length in each direction was initially set as half of the dimension of the simulation box in that direction, and was adjusted at the end of each cycle to give an acceptance ratio of 20%. The lengths of the simulation box in the *x*- and *y*-directions parallel to the graphite surface were 20 times the collision diameter of Kr

(0.3685 nm), and the dimension in the *z*-direction was 5 nm. The graphite surface was infinite in the *x* and *y* directions, and the uppermost graphene layer was positioned at $z = 0$ and a hard wall was positioned at $z = 5$nm.

3.2 Potential Energies

The interaction potential energies were assumed to be pairwise additive. The Kr-Kr interaction energy was described by a 12−6 Lennard-Jones (LJ) equation, with σ_{ff} =0.3685 nm and ε_{ff} / k_B =164.4 K[20]. The graphite surface was modelled as a structureless solid interacting with Kr atoms through a Steele 10-4-3 equation [21]. The carbon atom density of a graphene layer , ρ_s , was 38.2 /nm^2, and the molecular parameters for a carbon atom were, σ_{ss} = 0.3354 nm and ε_{ss} / k_B = 28 K. The cross collision diameter and the well-depth of the solid-fluid interactions were calculated by the Lorentz-Berthelot mixing rule.

3.3 Thermodynamic Properties

The surface excess concentration is defined as:

$$\Gamma_{ex} = \frac{N_{ex}}{L_x L_y} = \frac{\langle N \rangle - V\rho_G}{L_x L_y} \tag{2}$$

where N_{ex} is the excess amount adsorbed, $\langle N \rangle$ is the ensemble average of the number of particles in the simulation box, ρ_G is the bulk gas density, V is the accessible volume, L_x and L_y are the box dimensions in the *x*- and *y*-directions, respectively. The isosteric heat GCMC was calculated from fluctuation theory [22].

4. Results and Discussions

4.1 Krypton Adsorption on a Graphite Surface at 87.3 K

The experimental isotherm for krypton adsorption on Carbopack F at 87.3 K is shown in Figure 1. The step-wise layer by layer adsorption is characteristic of adsorption on a non-porous adsorbent [23] at temperatures below the bulk triple point (116 K for krypton). There is a steep transition at 1Pa to a low density monolayer followed by a gradual rise to an excess coverage of 10 μmol/m^2 at the point marked X on the inset. At about 700 Pa there is distinct vertical hysteresis loop (II in Figure 1) associated with the transition to second layer coverage, joining

two essentially horizontal hysteresis loops for the first layer (I) and second layer (III). Similar hysteresis loops were reported by Kosugi *et al.* [13] for temperatures in the range between 87 K and 116 K.

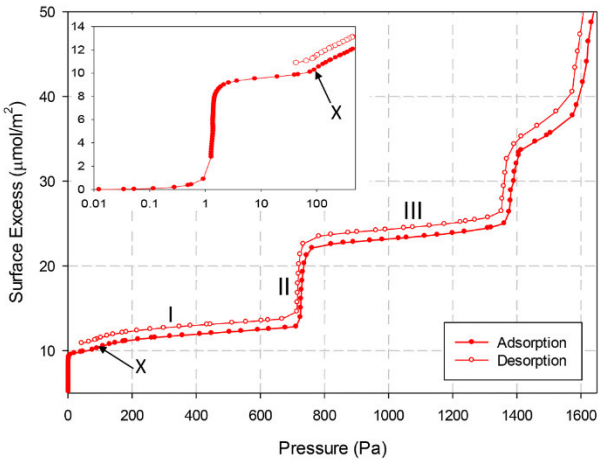

Figure 1 Experimental adsorption isotherm of Kr on Carbopack F at 87.3 K (P_0=1.7 kPa, desorption from 103 μmol/m^2).

The experimental isotherm is compared with the results from the simulations in Figure 2 and the isosteric heat curves are shown in Figure 3. The main features of the experimental result that are reproduced by the simulations are as follows:

i. There is a vertical transition (A-B) to a liquid-like monolayer at ~1Pa in both the experiment and the simulations as shown in Figure 2a.

ii. The simulations show two sub-steps at C and D in the first layer (Figure 2a), which have been widely reported experimentally [24-26] and are consistent with our previous work [1]. The gradual rise to the Point X in the experimental isotherm (Figure 1) corresponds to a similar rise to the Point D in the simulated isotherm (Figure 2a).

iii. The simulated isotherm shows a first order 2D-condensation (EF in Figure 2b) and evaporation (E'F') in the second layer, associated with the vertical and horizontal hysteresis loops, which also occur in the experimental data, but with a narrower hysteresis loop. The narrowing of the vertical hysteresis loop in the experimental result is possibly due to the geometrical constraint due to stacking of microcrystallites in Carbopack F, which we discuss in more detail in Section 4.3. This constraint becomes significant in higher layers, and for this reason that we shall restrict our comparison between the simulation results and the experimental data to the first two layers.

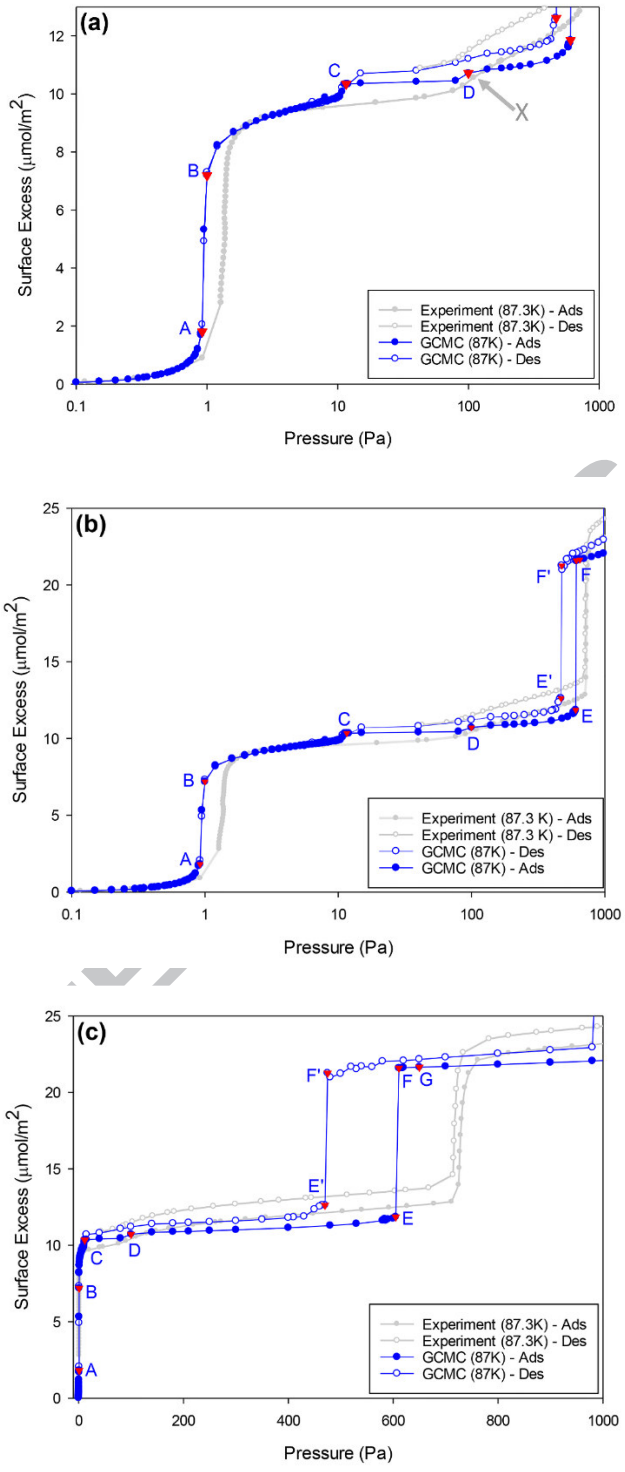

Figure 2- GCMC simulated adsorption isotherms of Kr on a structureless graphite at 87K and experimental isotherms of Kr on Carbopack F at 87.3 K: (a) enlargement of the monolayer adsorption isotherm plotted on a semi-logarithmic pressure scale, (b) adsorption isotherms up to second layer plotted on a semi-logarithmic pressure scale and (c) adsorption isotherms up to second layer plotted on a linear scale. The full adsorption isotherms are detailed in the Appendix.

To gain insight into the microscopic mechanism underlying the hysteresis, we first analyse the isosteric heat as a function of loading (Figure 3) along with the simulation snapshots for different loadings (Figure 4). The temperatures of the experimental isotherms (77.4K and 87.3K) are not close enough for an accurate calculation of the isosteric heat from the Clausius-Clapeyron equation, especially when coverage reaches the second and third layers, and we therefore expect no better than qualitative agreement between experiment and simulation. Nevertheless, the overall trends in the heat curve show good general agreement; for example both experiment and simulation exhibit a continuous increase in the first layer, followed by a very sharp decrease at the onset of the second layer and a constant heat across the 2D-transition in this layer.

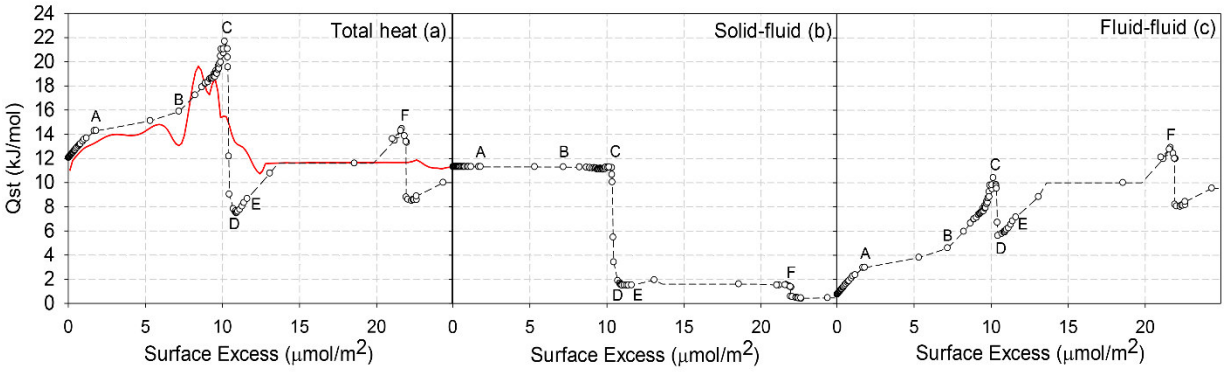

Figure 3-The isosteric heat versus loading for krypton adsorption on a structureless graphite obtained from GCMC at 87K (dashed line) and from experiments on Carbopack F at 77.4 K and 87.3 K (solid line). (b) and (c) are respectively: the Solid-Fluid and Fluid-Fluid contributions to the isosteric heat obtained with GCMC. Points A to F correspond to points marked on the adsorption isotherm in Figure 2.

The decomposition of the isosteric heats into contributions from the solid-fluid (SF) and fluid-fluid (FF) interactions are shown in Figure 3b and c. At zero loading, the isosteric heat of 12 kJ/mol, is solely due to the interaction between krypton and graphite and is in good agreement with the calculated value (12.03 kJ/mol) from direct Monte Carlo integration [27]. As the loading in the sub-monolayer coverage region is increased, the isosteric heat increases and reaches a maximum of about 22 kJ/mol when particles in the first layer form an almost perfect hexagonal packing (Point C), consistent with observations from our previous studies [28-29]. The additional 10 kJ/mol comes from the six nearest-neighbour krypton-krypton interactions, which each contribute approximately 1.37 kJ/mol together with contributions from neighbours in more distant shells (Point C of Figure 4), whilst the contribution from the SF interaction remains

constant (Figure 3b). At this stage (Point C), the first layer of Kr molecules acts like a quasi-surface for second-layer adsorption where an added krypton molecule interacts with three nearest-neighbour molecules in the first layer (see Point D of Figure 4). Therefore, the isosteric heat at the onset of second layer adsorption drops to a minimum of 8 kJ/mol, because there is a decrease in the number of nearest-neighbour Kr-Kr interactions (from six to three) and also because the Kr-graphite interaction is weaker since the second layer is further away from the graphite surface.

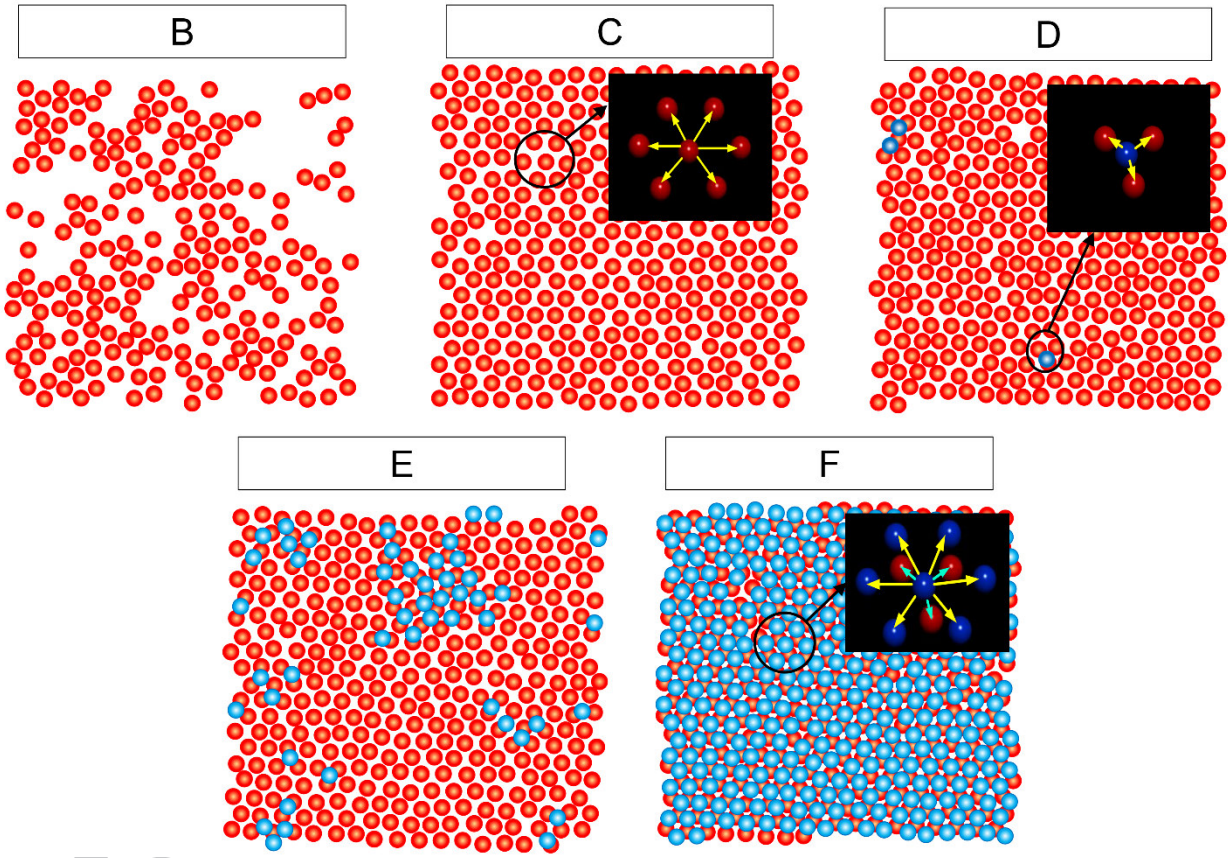

Figure 4-Snapshots (top view) of the simulated krypton adsorption on a structureless graphite surface at 87 K obtained from GCMC simulation. The krypton atoms in the first layer and second layers are shown as red and blue circles respectively (colour online). Points B to G correspond to points marked as B, C, D, E, F, G of Figure 2.

As more molecules are added in the second layer, the isosteric heat increases, due to interactions between the new molecule and existing molecules in the first and second layers. When the 2D transition occurs in the second layer, the isosteric heat remains constant at 12 kJ/mol, of which 2

kJ/mol comes from the SF interaction, as seen in Figure 2b and the remaining 10 kJ/mol from the FF interactions. This provides us with an excellent insight into how the 2D-condensation of the second layer proceeds; there are six nearest neighbour pair interactions and a contribution from neighbours in distant shells giving an equivalent of one 'extra' pair interaction. This comes mainly from the interaction of a new molecule with the first layer and with molecules in the second layer as its boundary grows.

The condensate in the second layer is initially liquid-like, but converts to hexagonal packing when further molecules are added. Each molecule resides on top of three molecules in the first layer and is surrounded by six molecules in the second layer (Point F in Figure 4), giving an isosteric heat contribution of ~12 kJ/mol as confirmed by the FF contribution to the total isosteric heat in Figure 3.

The boundary growth during the 2D transition of the second layer can be explained systematically by the 2D-density contours obtained from kMC simulations[30] in the canonical ensemble, previously studied fora monolayer of adsorbed argon below the 2D-critical temperature [31]. Figure 6 shows the 2D-density contour for the specific points marked in Figure 5. At the spinodal Point 1, a patch of liquid-like krypton is present and grows to form a strip at Point 2. With further increase in loading, the strip expands at the expense of the rarefied phase (Point 3) and eventually the second layer becomes fully covered with solid-like krypton at spinodal Point 4.

The NVT-kMC simulation also sheds some light on the hysteresis in krypton adsorption on graphite. In Figure 6, the canonical isotherm exhibits a van der Waals-type loop with a vertical section that is associated with a two phase coexistence region, as noted in our earlier work at 73 K [1], which confirms the second layer hysteresis obtained with GCMC. The NVT-kMC simulation also substantiates the presence of a horizontal hysteresis loop, noting that the canonical isotherm fits in between the adsorption-desorption branch in the horizontal hysteresis loop region.

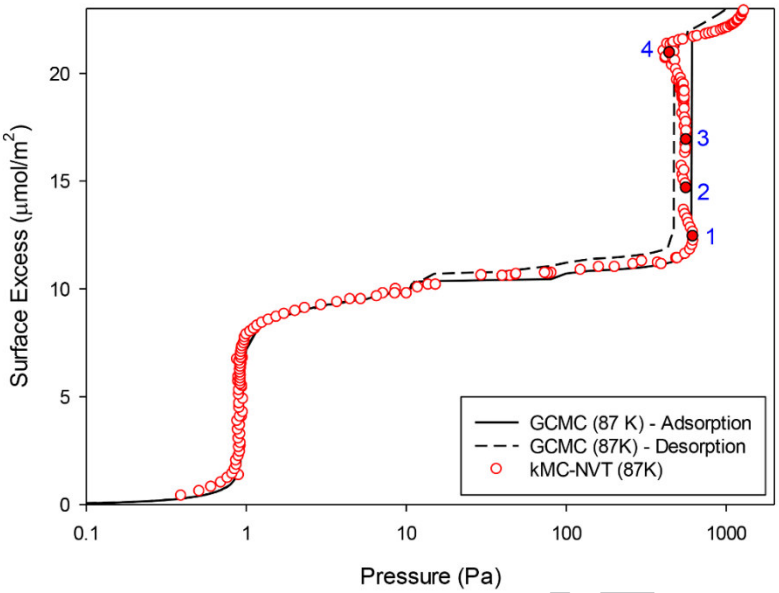

Figure 5-The adsorption isotherms of Kr on a graphite surface at 87 K: comparison between the results of GCMC and kMC-NVT. The kMC-NVT simulation was made on a rectangular infinite graphitic surface of 30 σ_{ff} ×10σ_{ff} and generated with 5 × 10^7 configurations for both equilibrium and sampling stages.

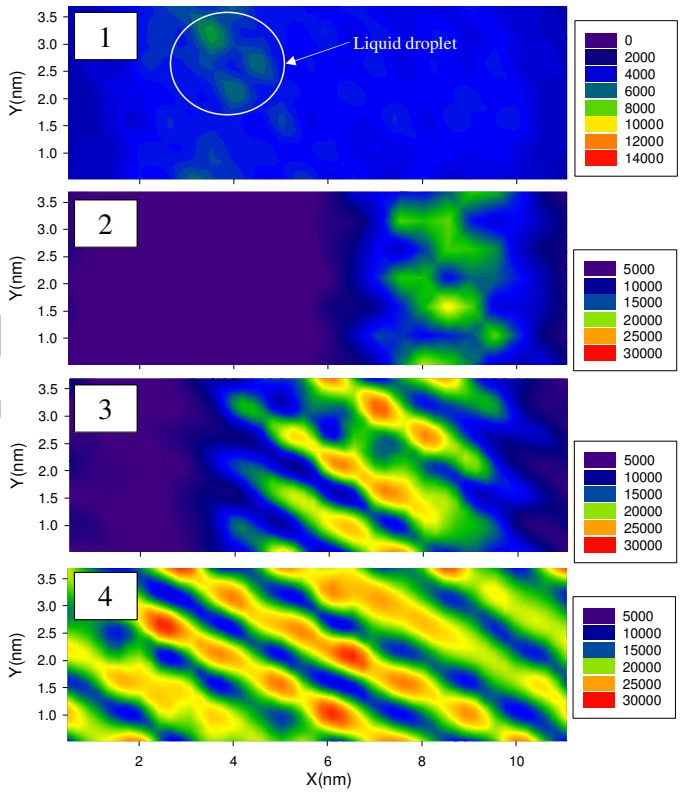

Figure 6-2D density plots of second layer Kr adsorption on a rectangular infinite graphitic surface of 30 σ_{ff} ×10σ_{ff} at 87K from kMC simulation (colour online). Points 1,2,3 and 4 correspond to points marked in Figure 5.

4.1.1 Local Properties Analysis

Our recent study [1] suggests that the microscopic reason for the hysteresis lies in the restructuring and progressive cohesiveness of the adsorbate as loading increases. In this section we corroborate this argument by analysing the local density profiles at different stages in the adsorption (Figure 7) and the compressibility of the first and second layers as a function of pressure (Figure 9).

Local Density Distribution

The distinct peaks in the local density profile demonstrate the layering mechanism. After formation of the first layer to a liquid-like state (Point B), there is a small vertical sub-step in the isotherm at Point C, which signals the transition from the liquid-like state to an imperfect solid-like state. The second vertical sub-step at Point D corresponds to further densification of the first layer, and this imperfectly ordered state in the first layer remains stable until Point E, just before the 2D-condensation to the second layer. The changes of the state in the first adsorbed layer at these points can be seen in the 2D-density contour plots given in the Appendix. The most interesting feature from the analysis of the local density distributions is that, when the condensation of the second layer occurs, there is a small but distinct transition in the density of the first layer (From Point F to G), which is associated with the further densification of this layer to an hexagonally packed 2D solid-like state.

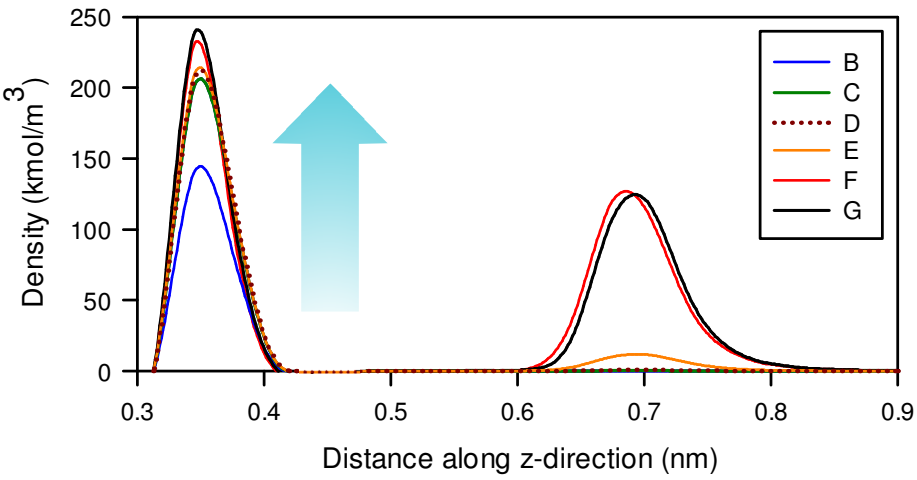

Figure 7- Local density profiles along the z-direction for Kr adsorption on graphite at 87 K obtained from GCMC (colour online). Plots B to G correspond to points marked as B, C, D, E, F, G of Figure 2.

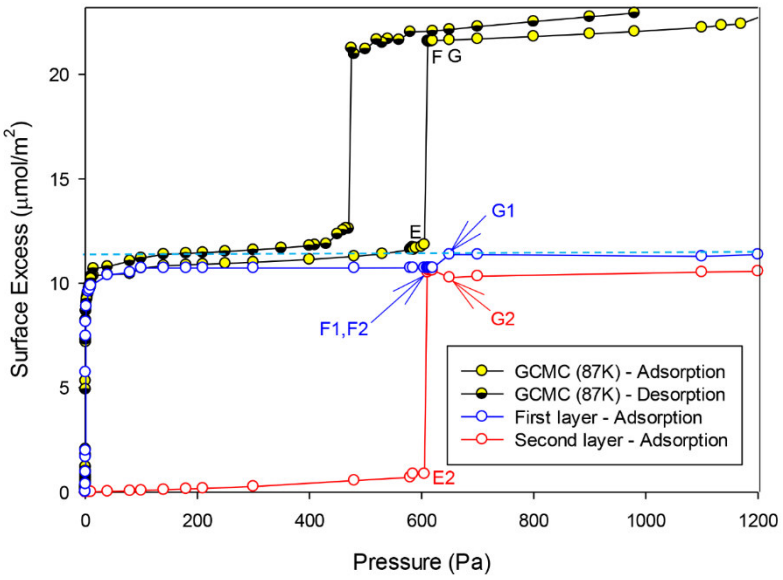

Figure 8-Decomposition of the GCMC adsorption isotherm for Kr adsorption at 87K on a structureless graphite surface into first and second layer coverage plotted on a linear scale.

This is supported by decomposing the isotherm into first and second layer contributions as shown in Figure 8. This decomposition demonstrates that, while the total amount adsorbed is conserved from Point F to Point G, the amount adsorbed in the second layer (Point G2) decreases as the coverage in the first layer increases (Point G1). Over the same pressure range (from Point F to G), the total density remains constant, which means that the increase in the first layer density comes about at the expense of a decrease in the second layer density (see Figure 8), indicating that molecules are transferred between the two layers. This observation emphasizes a point that has not been well recognized in previous literature, namely: that lower layers may be continuously compressed by addition to higher layers, and that at temperatures below the triple point, a nearly perfect 2D solid may be formed, as is the case in this system.

Local Compressibility

The compressibility is defined as the negative of the relative change of relative volume with pressure at constant temperature

$$\kappa = -\frac{1}{V}\left(\frac{\partial V}{\partial P}\right)_T \qquad (3)$$

and is related to the particle number fluctuation [22] by,

$$\frac{k_B T}{V}\kappa = \frac{< N^2 > - < N >^2}{< N >^2} \qquad (4)$$

which is also a measure of the transferability of molecules within a system.

Figure 9 shows the local compressibility in the first and second layers: the compressibility of the first layer is significantly lower because the layer is held strongly to the surface by the adsorption forces, and has a high density. The first sharp decrease in compressibility corresponds to the change to a liquid-like state at B. The compressibility of the first layer reaches that of the bulk Kr solid at C, the first vertical sub-step in the simulated isotherm, but the compressibility of the first and second layers continue to decrease with increasing pressure.

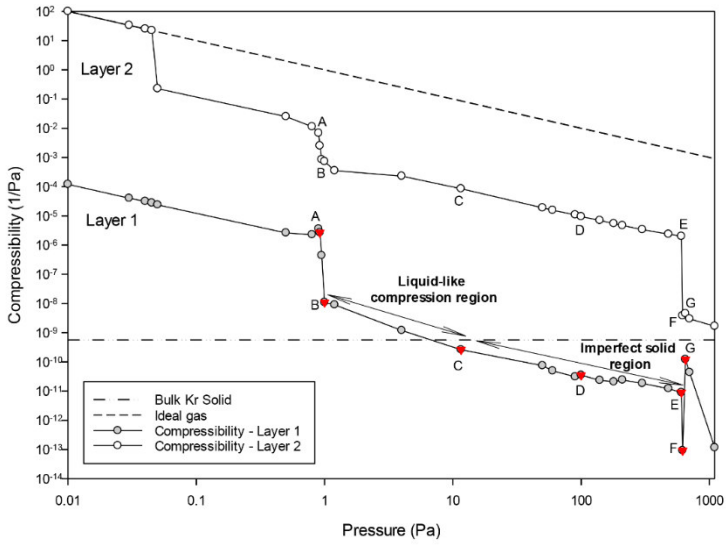

Figure 9 - Layer compressibility of the first and second layers during Kr adsorption on a structureless graphite at 87 K obtained from GCMC.

When the 2D-condensation occurs in the second layer there is a corresponding sharp decrease in the compressibility in the second layer and in the first layer (Point E to Point F). This is again indicative of the fact that a large addition of molecules into the second layer exerts some degree of compression on the first layer inducing a solid-like state. At Point G, when some molecules from the second layer squeeze into the first layer, there is an increase in the compressibility of the first layer that can be attributed to the entry of molecules into the first layer. There is apparently no noticeable change in the compressibility of the second layer at point G. This is because the second layer is still in a liquid-like state, and a small change in the number

fluctuation in the second layer cannot be detected because the compressibility of the second layer is two orders of magnitude greater than that of the first layer.

Nevertheless, the first layer compressibility at G is still below that of bulk Kr solid and this supports our earlier assertion that when 2D condensation occurs in the second layer the first layer becomes denser, changing from an dense disordered state to a compressed solid-like state. This is clear evidence of adsorbate compression, and it is this phenomenon that gives rise to the hysteresis because the pressure must be reduced to a lower value before the adsorbed layer can evaporate, giving rise to a horizontal hysteresis loop after the evaporation of the second layer. When desorption is carried out from two filled layers, there is a vertical hysteresis associated with the evaporation of the second layer, but the desorption branch does not join the adsorption branch; instead the density decreases until it coincides with that of the solid-like state of the first layer (at Point G – see dashed line in Figure 8). A lower pressure is then required to bring it to a less perfect solid-like state, resulting in a horizontal hysteresis loop; a feature that has not been reported previously in the literature. The horizontal hysteresis loop eventually closes after Point C, when the compressibility of the adsorbed first layer has decreased to that of a liquid state. We can conclude that the hysteresis loop is caused by an irreversible compression of the first layer, resulting from squeezing in of molecules from the second layer after the 2D-condensation, as the first layer orders into a solid-like state such that desorption to bring it back into a liquid-like state requires a pressure lower than the condensation pressure.

Effect of Repulsion on Local Compressibility

The 12-6 Lennard-Jones (LJ) pairwise potential and the corresponding Steele 10-4-3 potential are used in this study to generate the GCMC adsorption/desorption isotherm. These potentials are widely used to describe the fluid-fluid and solid-fluid interaction in adsorption studies although it is well-known that the inverse 12th-power repulsive term in the LJ model is empirical. In this section, we investigate the effect of the repulsion on compressibility by modifying the pairwise potential energy between LJ sites (φ_{ff}) to have a shallower repulsion (10-6 potential) or a steeper repulsion (18-6 potential). The potential energy of an LJ site with a structureless surface (φ_{sf}) is modified accordingly to give an 8-4 potential or 16-4 potential as shown in Eq. (5)-(8) (plotted in Figure 10). The derivation of these equations is provided in the supporting information.

The φ_{ff} and φ_{sf} for the 10-6 Potential is given by:

$$\varphi_{ff} = \frac{25\sqrt{5}}{6\sqrt{3}}\varepsilon_{ff}\left[\left(\frac{\sigma_{ff}}{r}\right)^{10} - \left(\frac{\sigma_{ff}}{r}\right)^{6}\right] \tag{5}$$

$$\varphi_{sf} = \frac{25\pi\sqrt{5}}{12\sqrt{3}}\sigma_{sf}{}^{2}\rho_{s}\varepsilon_{sf}\left\{\left[\frac{1}{2}\left(\frac{\sigma_{sf}}{z}\right)^{8} - \left(\frac{\sigma_{sf}}{z}\right)^{4}\right] + \left[\frac{1}{2}\left(\frac{\sigma_{sf}}{z+\Delta}\right)^{8} - \left(\frac{\sigma_{sf}}{z+\Delta}\right)^{4}\right] + \left[\frac{1}{2}\left(\frac{\sigma_{sf}}{z+2\Delta}\right)^{8} - \left(\frac{\sigma_{sf}}{z+2\Delta}\right)^{4}\right]\right\} \tag{6}$$

And for the 18-6 Potential is given by,

$$\varphi_{ff} = \frac{3\sqrt{3}}{2}\varepsilon_{ff}\left[\left(\frac{\sigma_{ff}}{r}\right)^{18} - \left(\frac{\sigma_{ff}}{r}\right)^{6}\right] \tag{7}$$

$$\varphi_{sf} = \frac{3\pi\sqrt{3}}{4}\sigma_{sf}{}^{2}\rho_{s}\varepsilon_{sf}\left\{\left[\frac{1}{4}\left(\frac{\sigma_{sf}}{z}\right)^{16} - \left(\frac{\sigma_{sf}}{z}\right)^{4}\right] + \left[\frac{1}{4}\left(\frac{\sigma_{sf}}{z+\Delta}\right)^{16} - \left(\frac{\sigma_{sf}}{z+\Delta}\right)^{4}\right] + \left[\frac{1}{4}\left(\frac{\sigma_{sf}}{z+2\Delta}\right)^{16} - \left(\frac{\sigma_{sf}}{z+2\Delta}\right)^{4}\right]\right\} \tag{8}$$

Where r is the separation distance between two particles, z is the distance between the fluid particle and the graphite layer and Δ is the spacing between two adjacent graphite layers. The solid-fluid molecular parameters: the collision diameter σ_{sf} and the interaction energy ε_{sf} are calculated from the Lorentz-Berthelot mixing rule.

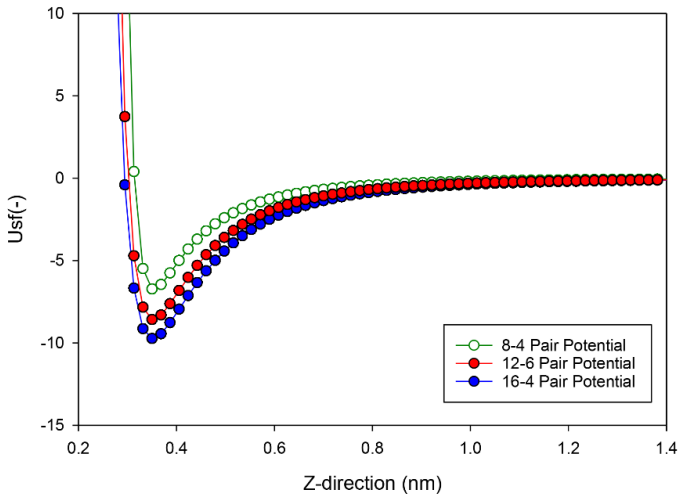

Figure 10- Modified solid-fluid potentials normal to the surface derived for the 8-4, 16-4 and 12-6 (to give the standard 10-4-3 model) pair potentials.

The adsorption isotherms for the 10-6 and 18-6 pair potentials are shown in Figure 11a and a number of observations can be made from this plot:

1. It is evident that up to monolayer coverage, the adsorbate densities for the three cases are at the same level (see the lower dashed line in Figure 11a).
2. The 2D transition in the first layer is observed for the 10-6 Potential at Point A' to B' but disappears when the repulsive interaction is increased. There are still two distinct substeps for the shallower repulsion (10-6) but these become less apparent for the steeper repulsion, and only one substep was found for the 18-6 potential. These observations are similar to the effects of increasing temperature, as studied previously [1].

The effect of the repulsive interaction on local compressibility is also evident in Figure 11b and some interesting features are as follows:

1. The compressibility of the 10-6 adsorbate is lower than that of the 12-6 adsorbate as the weaker repulsion corresponds to less fluctuation because the attraction between the molecules and between the adsorbate and the structureless solid is relatively weaker. Similarly, the stronger repulsive interaction in 18-6 potential corresponds to a higher compressibility as the adsorbed molecules are in a less cohesive state.
2. The compressibility drops sharply during the phase change (A' to B' and A'' to B'') and 2D condensation (E' to F'), as expected.

The aforementioned observations indicate that the repulsive interaction plays a significant role in the simulated adsorption isotherm and local compressibility. The role of the repulsive term in the potential equation might also be the reason for the discrepancies between simulation and experiment because of the deficiencies of the 12-6 Lennard Jones and 10-4-3 potentials. Nevertheless, the progressive compression as adsorption proceeds for all three potential models is clearly evident and therefore supports the view that adsorbate compression is the origin of the observed hysteresis.

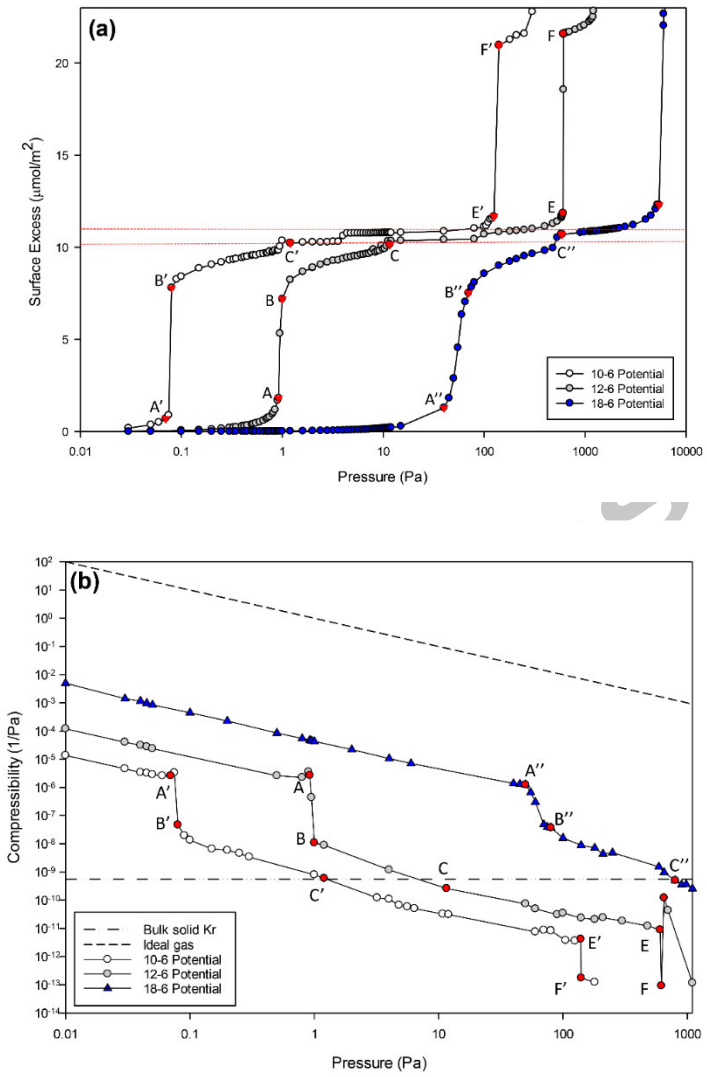

Figure 11- (a) Adsorption isotherms for Kr adsorption on a structureless graphite at 87 K for 10-6, 12-6 and 18-6 potentials obtained from GCMC,(b) local compressibilities in the first adsorbed layer, for 10-6, 12-6 and 18-6 potentials

4.2 Geometrical Factors

Other artefacts in a real solid adsorbent may affect surface adsorption. One such factor is that Carbopack F has narrow interstices between the micro-crystallites of the adsorbent. The enhanced potential field in the microporous spaces at these junctions means that adsorption there may proceed by micropore filling, which could contribute significantly to the overall isotherm, but would not show hysteresis if the pores are of micropore width. The geometrical constraint caused by stacking of the microcrystallites may also become significant in higher layers, and for this reason we have restricted our study to data from the first two adsorbed layers.

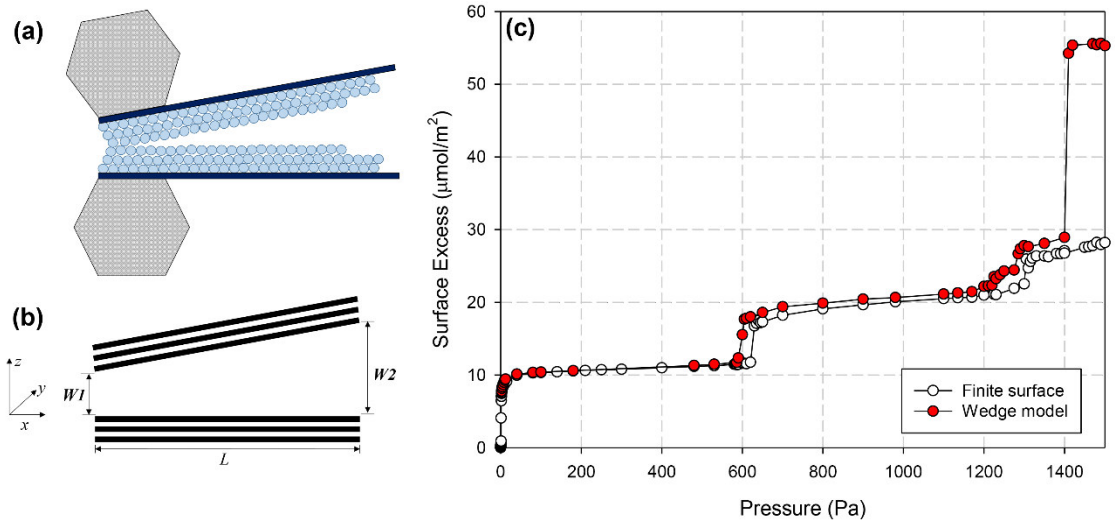

Figure 12-(a) Illustration of interstices formed between two graphite surfaces, (b) schematics of the wedge pore model using three Bojan-Steele layers for each wall, (c) adsorption isotherm for krypton at 87 K on a 20σff × 20σff Bojan-Steele surface (empty symbols) and on a wedge pore model with L= 10nm, W1=3.33nm, W2=4.53nm (filled symbols). The size of each graphite layer of the wedge pore model is 10σff × 10σff. 100,000 cycles were run for both equilibrium and sampling stages for both surface and wedge pore model.

To evaluate the effect of crevice micropores we carried out simulations of krypton adsorption in a wedge shaped confined space as a model for these interstices. Figure 12 shows the adsorption isotherm for this model, together with the isotherm for the perfect graphite, discussed in earlier sections. The two isotherms agree for adsorption up to the first two layers, then interference from the junction begins to exert its influence in the third and higher layers, resulting in a more gradual change in density in the third layer, in better agreement with the experimental data. The isotherm for the perfect graphite on the other hand, exhibits a steep change in density when coverage reaches the third layer. This is consistent with our analysis of adsorbate compression and hysteresis in the first and second layers, and supports our argument that the reason for the hysteresis observed in the first two layers is adsorbate compression, rather than interference by capillary condensation.

5. Conclusion

Krypton adsorption on non-porous graphite at 87K (below the bulk triple point of krypton) has been found in previous work, to exhibit second layer hysteresis, contrary to the conventional view that hysteresis is only associated with condensation and evaporation in mesopores. In this study, we have confirmed this observation by experiments on Carbopack F (a non-porous carbon adsorbent) supported by GCMC simulation. Analysis of local properties indicates that the continuous densification and ordering of the adsorbate, especially in the first layer, as adsorption proceeds in higher layers, is the primary reason for the hysteresis. We also find a horizontal hysteresis loop in the first layer, both experimentally and in simulation, which we attribute to the development of a solid-like state in this layer when the second layer condenses and molecules migrate from the second layer into the first layer. This mechanism does not appear to have been previously recognized in the literature.

Acknowledgments

This project is supported by the Australian Research Council, DP160103540

Appendix

Full Adsorption Isotherm

Figure A1 shows the full adsorption isotherm for krypton at 87K up to the condensation pressure, obtained with GCMC on a continuum model graphite and experiments on Carbopack F. In the simulations desorption was from a coverage of 46 µmol/m^2 and in the experiments from 103 µmol/m^2. It should be noted that the 87.3K experimental isotherm matches better with a simulated isotherm at 88.5K (Figure A1(b)).

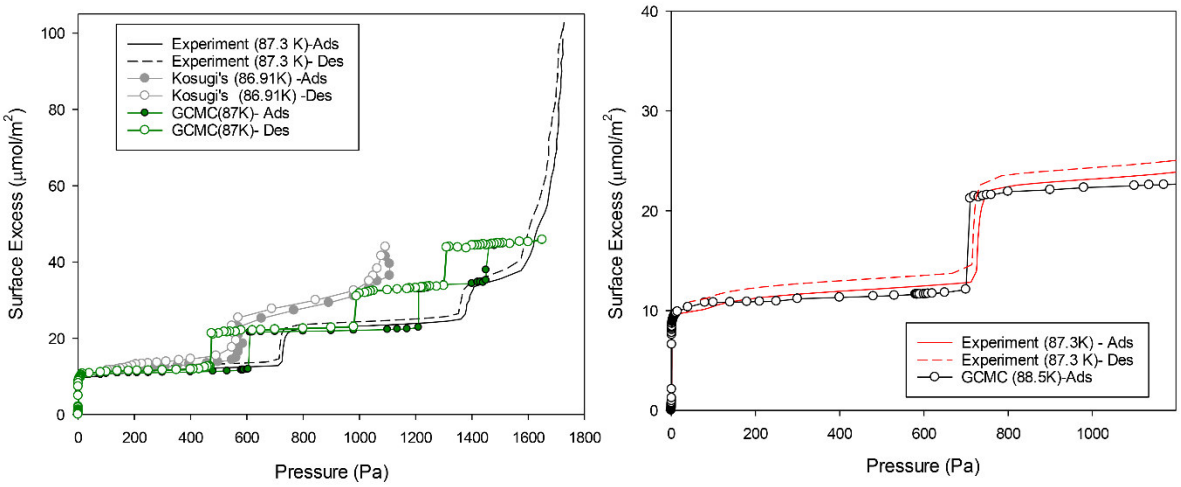

Figure A1-Adsorption isotherm for krypton on a structureless graphite obtained from GCMC: (a) at 87 K and (b) at 88.5K with the superimposed experimental data.

Effects of Temperatures

Figure A2 shows simulated isotherms for krypton at higher temperatures. In general the sharp multilayer steps and area of the hysteresis loop diminish with increasing temperature due to the increased thermal motion of the molecules. At 116K (bulk triple point of krypton), GCMC gives a completely reversible isotherm. This is in contrast with the experiments on an exfoliated graphite adsorbent reported by Kosugi et al., where hysteresis was found to occur at 116K. Despite the general agreement between our simulation and their data,we suggest that this difference is due to capillary condensation in spaces between graphite platelets. At this temperature our simulations did not show any 2D-condensation or constant heat regions. At 120 K (boiling point of krypton), both simulation and Kosugi's data show no hysteresis. The reversibility of krypton adsorption at temperatures above 94.72K was also observed by Putnam and Fort [32]. Hysteresis below 87K in GCMC simulation were reported by Rui et al[1].

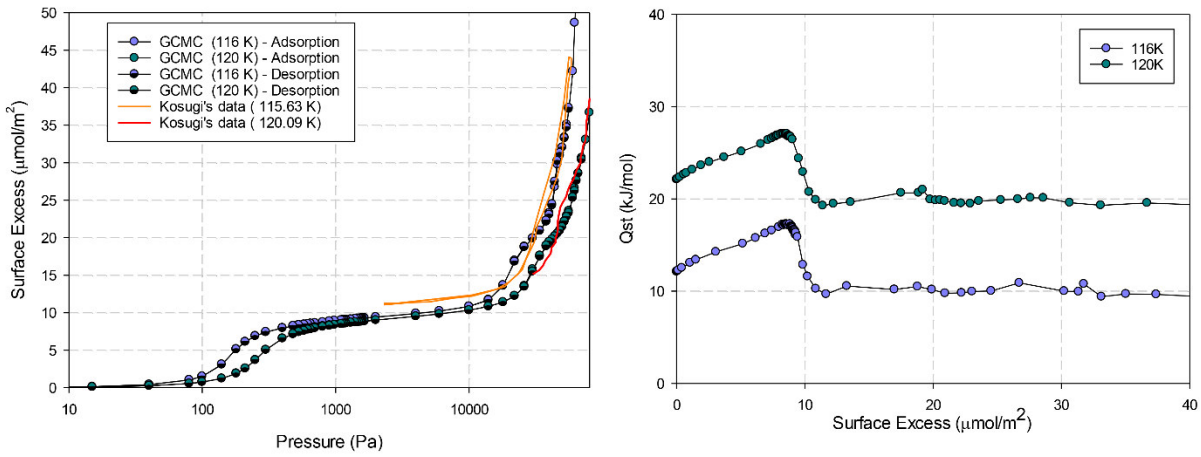

Figure A2- (a) GCMC adsorption isotherm for Kr at 116K and 120K (b) GCMC isosteric heat curves for 116 K and 120K. The curve for 120K is shifted by 10 kJ/mol (colour online).

2D-Density Contours

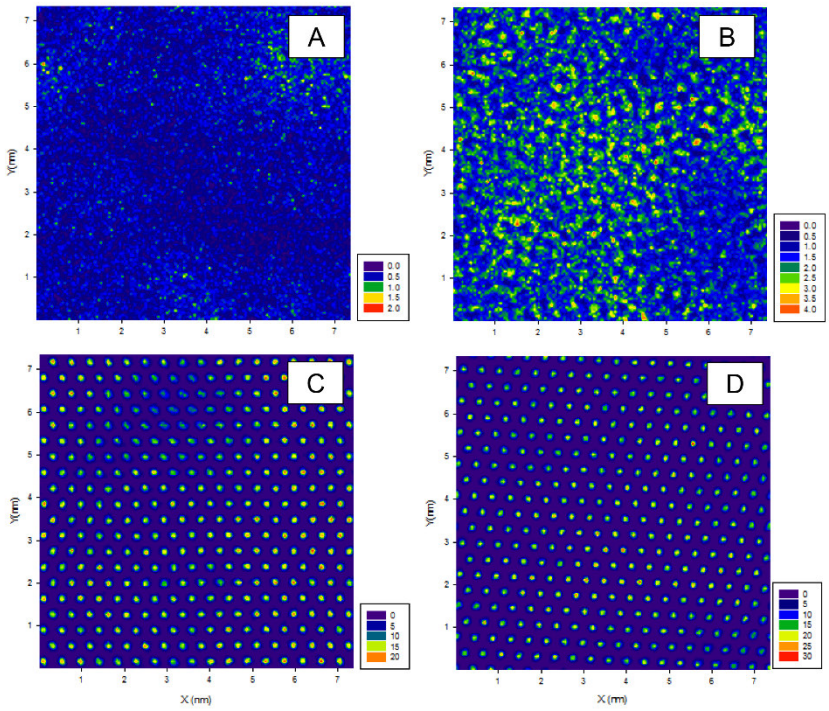

Figure A3-2D-density contours (colour online) for Kr adsorbed on a graphite surface at 87K. A-D correspond to the points A, B, C, D in Figure 2 showing the change in the first layer from a gas-like state (Point A) to a liquid-like state at B through an imperfect solid-like state (Point C) to a more densified state at Point D.

References

1. Diao, R.; Fan, C.; Do, D.; Nicholson, D., On the 2d-Transition, Hysteresis and Thermodynamic Equilibrium of Kr Adsorption on a Graphite Surface. *Journal of Colloid and Interface Science* **2015**, *460*, 281-289.
2. Thommes, M.; Kaneko, K.; Neimark, A. V.; Olivier, J. P.; Rodriguez-Reinoso, F.; Rouquerol, J.; Sing, K. S., Physisorption of Gases, with Special Reference to the Evaluation of Surface Area and Pore Size Distribution (IUPAC Technical Report). *Pure and Applied Chemistry* **2015**, *87*, 1051-1069.
3. Prenzlow, C. F.; Halsey, G. D., Argon-Xenon Layer Formation on Graphitized Carbon Black from 65 to 80â°K. *The Journal of Physical Chemistry* **1957**, *61*, 1158-1165.
4. Amberg, C. H.; Spencer, W. B.; Beebe, R. A., Heats of Adsorption of Krypton on Highly Graphitized Carbon Black. *Canadian Journal of Chemistry-Revue Canadienne De Chimie* **1955**, *33*, 305-313.
5. Avgul, N. N.; Kiselev, A. V., Physical Adsorption of Gases and Vapous on Graphitized Carbon Blacks. *Chemistry and Physics of Carbon* **1970**, *6*, 1 - 124.
6. Polley, M. H.; Schaeffer, W. D.; Smith, W. R., Development of Stepwise Isotherms on Carbon Black Surfaces. *Journal of Physical Chemistry* **1953**, *57*, 469-471.
7. Gardner, L.; Kruk, M.; Jaroniec, M., Reference Data for Argon Adsorption on Graphitized and Nongraphitized Carbon Blacks. . *Journal of Physical Chemistry B* **2001**, *105*, 12516-12523.
8. Dell, R. M.; Beebe, R. A., Heats of Adsorption of Polar Molecules on Carbon Surfaces .2. Ammonia and Methylamine. *Journal of Physical Chemistry* **1955**, *59*, 754-762.
9. Holmes, J. M.; Beebe, R. A., An Example of Desorption Hysteresis at Low Relative Pressure on a Non-Porous Adsorbent - Ammonia on Graphitized Carbon Black. *Journal of Physical Chemistry* **1957**, *61*, 1684-1686.
10. Inaba, A.; Koga, Y.; Morrison, J. A., Multilayers of Methane Adsorbed on Graphite. *Journal of the Chemical Society, Faraday Transactions 2: Molecular and Chemical Physics* **1986**, *82*, 1635-1646.
11. Lysek, M. J.; LaMadrid, M.; Day, P.; Goodstein, D., Adsorption Hysteresis, Capillary Condensation and Melting in Multilayer Methane Films on Graphite Foam. *Langmuir* **1992**, *8*, 898-900.
12. Larher, Y.; Angerand, F.; Maurice, Y., Wetting of Graphite (0001) by Carbon Monoxide. A Stepwise Adsorption Isotherm Study. *Journal of the Chemical Society, Faraday Transactions 1: Physical Chemistry in Condensed Phases* **1987**, *83*, 3355-3366.
13. Kosugi, T.; Usui, Y.; Arakawa, I. In *Adsorption-Desorption Hysteresis in the Adsorption-Isotherms for Kr and Xe on Exfoliated Graphite*, The Hague, Netherlands, Oct 12-16; The Hague, Netherlands, 1992; pp 862-865.
14. Morishige, K.; Kawamura, K.; Yamamoto, M.; Ohfuji, I., Capillary Condensation of Xe on Exfoliated Graphite. *Langmuir* **1990**, *6*, 1417-1421.
15. Kruchten, F.; Knorr, K., Multilayer Adsorption and Wetting of Acetone on Graphite. *Physical Review Letters* **2003**, *91*.
16. Bah, A.; Dupont-Pavlovsky, N.; Duval, X., Adsorption Hysteresis and 2d Phase Nucleation of Chloroform on Graphite. *Surface science* **1996**, *352*, 518-522.
17. Horikawa, T.; Zeng, Y.; Do, D.; Sotowa, K.-I.; Avila, J. R. A., On the Isosteric Heat of Adsorption of Non-Polar and Polar Fluids on Highly Graphitized Carbon Black. *Journal of colloid and interface science* **2015**, *439*, 1-6.

18. Horikawa, T.; Takenouchi, M.; Do, D. D.; Sotowa, K.-I.; Alcántara-Avila, J. R.; Nicholson, D., Adsorption of Water and Methanol on Highly Graphitized Thermal Carbon Black and Activated Carbon Fibre. *Australian Journal of Chemistry* **2015**, *68*, 1336-1341.
19. Horikawa, T.; Muguruma, T.; Do, D.; Sotowa, K.-I.; Alcántara-Avila, J. R., Scanning Curves of Water Adsorption on Graphitized Thermal Carbon Black and Ordered Mesoporous Carbon. *Carbon* **2015**, *95*, 137-143.
20. Maitland, G. C.; Rigby, M.; Smith, E. B.; Wakeham, W. A., *Intermolecular Forces. Their Origin and Determination*; Oxford Science Publications: Oxford, 1987, p xiv. 616.
21. Steele, W. A., The Physical Interaction of Gases with Crystalline Solids: I. Gas-Solid Energies and Properties of Isolated Adsorbed Atoms. *Surface Science* **1973**, *36*, 317-352.
22. Nicholson, D.; Parsonage, G., *Computer Simulation and the Statistical Mechanics of Adsorption*; Academic Press: London, 1982.
23. Thomy, A.; Duval, X., Adsorption of Simple Molecules on Graphite.2. Variation of Adsorption Potential as Function of Number of Adsorbed Layers. *Journal De Chimie Physique Et De Physico-Chimie Biologique* **1970**, *67*, 286-&.
24. Duval, X.; Thomy, A., The Interpretation of Krypton Adsorption Isotherms on Exfoliated Graphite. *Carbon* **1975**, *13*, 242-243.
25. Larher, Y., Triple Point of First Monomolecular Layer of Krypton Adsorbed on the Cleavage Face of Graphite. *Journal of the Chemical Society-Faraday Transactions I* **1974**, *70*, 320-329.
26. Larher, Y.; Terlain, A., Transition from Fluid to Registered Solid of the Krypton Monolayer Adsorbed on the Basal Face of Graphite. *The Journal of Chemical Physics* **1980**, *72*, 1052-1054.
27. Do, D.; Nicholson, D.; Do, H., On the Henry Constant and Isosteric Heat at Zero Loading in Gas Phase Adsorption. *Journal of colloid and interface science* **2008**, *324*, 15-24.
28. Nguyen, V. T.; Do, D. D.; Nicholson, D., On the Heat of Adsorption at Layering Transitions in Adsorption of Noble Gases and Nitrogen on Graphite. *The Journal of Physical Chemistry C* **2010**, *114*, 22171-22180.
29. Wang, Y.; Razak, M. A.; Do, D.; Horikawa, T.; Morishige, K.; Nicholson, D., A Computer Simulation and Experimental Study of the Difference between Krypton Adsorption on a Graphite Surface and in a Graphitic Hexagonal Pore. *Carbon* **2012**, *50*, 2908-2917.
30. Fan, C.; Do, D.; Nicholson, D., The Concept of Mean Free Path in the Kinetic Monte Carlo Description of Bulk Fluid Behaviour, Vapour–Liquid Equilibria and Surface Adsorption of Argon. *Molecular Simulation* **2012**, *38*, 1001-1009.
31. Phadungbut, P.; Nguyen, V. T.; Do, D.; Nicholson, D.; Tangsathitkulchai, C., On the Phase Transition in a Monolayer Adsorbed on Graphite at Temperatures Below the 2d-Critical Temperature. *Molecular Simulation* **2015**, *41*, 446-454.
32. Putnam, F. A.; Fort Jr, T., Physical Adsorption of Patchwise Heterogeneous Surfaces. I. Heterogeneity, Two-Dimensional Phase Transitions, and Spreading Pressure of the Krypton-Graphitized Carbon Black System near 100. Deg. K. *The Journal of Physical Chemistry* **1975**, *79*, 459-467.